ENGINEERING

# An antibody-based molecular switch for continuous small-molecule biosensing

**Ian A.P. Thompson[1], Jason Saunders[1], Liwei Zheng[2], Amani A. Hariri[2], Nicolò Maganzini[1], Alyssa P. Cartwright[1], Jing Pan[3], Steven Yee[1], Constantin Dory[1], Michael Eisenstein[1,2], Jelena Vuckovic[1], Hyongsok Tom Soh[1,2]***



**We present a generalizable approach for designing biosensors that can continuously detect small-molecule biomarkers in real time and without sample preparation. This is achieved by converting existing antibodies into target-responsive "antibody-switches" that enable continuous optical biosensing. To engineer these switches, antibodies are linked to a molecular competitor through a DNA scaffold, such that competitive target binding induces scaffold switching and fluorescent signaling of changing target concentrations. As a demonstration, we designed antibody-switches that achieve rapid, sample preparation–free sensing of digoxigenin and cortisol in undiluted plasma. We showed that, by substituting the molecular competitor, we can further modulate the sensitivity of our cortisol switch to achieve detection at concentrations spanning 3.3 nanomolar to 3.3 millimolar. Last, we integrated this switch with a fiber optic sensor to achieve continuous sensing of cortisol in a buffer and blood with <5-min time resolution. We believe that this modular sensor design can enable continuous biosensor development for many biomarkers.**

## INTRODUCTION

Sensors capable of continuously measuring molecular analytes in a compact format offer tremendous potential in personalized health monitoring (*1*–*5*), early disease detection (*6*, *7*), and inpatient care (*8*). A few such continuous biosensors have been developed to date and now play a critical role in modern medicine. Continuous glucose monitors (CGMs) have revolutionized diabetes management by enabling long-term monitoring of a patient's glycemic control and generating real-time alerts for rapid intervention (*9*, *10*), and pulse oximetry has become an essential tool for directly measuring blood oxygenation during critical care (*11*). However, both of these technologies rely on analyte-specific sensing mechanisms; the former uses a glucose-specific enzyme that produces redox-active species (*12*), whereas the latter relies on the intrinsic optical properties of oxygenated blood (*13*). Hence, there is a considerable opportunity for more generalizable biosensor frameworks that can readily be adapted to recognize a broad spectrum of clinically important biomarkers. This will require the development of new continuous molecular detection strategies that can be rapidly and reliably adapted to many different biochemical targets.

Designing such a "universal" continuous biosensing mechanism presents a tremendous technological challenge. The sensing mechanism must achieve rapid, sensitive, and specific molecular recognition that generates a measurable signal output—ideally, using readily available affinity reagents as building blocks. To operate continuously at the point of care, sensing should also require minimal to no sample preparation or additional reagents to achieve detection. Switch-based biosensors have emerged as a promising solution that combines molecular recognition and signaling capabilities within a single receptor to enable continuous sensing without the need for additional reagents (*14*). To date, these biosensors have primarily used sensor surfaces functionalized with DNA-based aptamer switches that change their conformation upon binding to a target, thereby enabling sensing through electrochemical or fluorescent reporters coupled to the DNA sequence. Aptamer switches have been applied to sensing a range of targets (*15*–*20*), but they remain difficult to generalize. This is partly because there is only a limited pool of high-performance aptamers available, such that each additional aptamer-based sensor requires the selection of an additional aptamer that binds the relevant analyte with excellent affinity and specificity (*21*). In many cases, these newly selected aptamers must be further engineered to ensure that they undergo binding-induced conformational switching to generate a measurable signal (*22*). Both of these processes are laborious and unpredictable in terms of success rates, and thus, the use of aptamer switch-based biosensors has remained limited to sensing a relatively small number of important biomarkers. Two recently described promising approaches to sensing have instead leveraged antibodies as receptors for detecting protein biomarkers, demonstrating high sensitivity and good generalizability (*23*, *24*). However, these approaches rely on either large mass changes upon binding or two-epitope recognition and thus are unsuitable for detecting the broad range of clinically important small-molecule biomarkers including drugs, metabolites, and hormones. Hence, there remains an unmet need for robust and generalizable strategies for developing molecular switches that can greatly expand the range of continuous biosensing applications for small-molecule analytes.

To this end, we have developed a strategy for adapting existing antibodies into "antibody-switches" that can achieve continuous detection of small molecules. Antibodies present an attractive alternative to aptamers as they are broadly available for a wide range of targets and offer a conserved, predictable structure that should make a generalizable engineering strategy feasible. In our antibody-switch design, an antibody is site-specifically augmented with a DNA scaffold to form a chimeric molecule that undergoes

[1]Department of Electrical Engineering, Stanford University, Stanford, CA 94305, USA. [2]Department of Radiology, Stanford University, Stanford, CA 94305, USA. [3]Department of Mechanical and Aerospace Engineering, Herbert Wertheim College of Engineering, University of Florida, Gainesville, FL 32611, USA.
*Corresponding author. Email: tsoh@stanford.edu

target-responsive switching upon antibody-antigen binding. This switching occurs through intramolecular competitive binding between the target antigen and a molecular "bait" linked to the end of the DNA scaffold. By introducing a Förster resonance energy transfer (FRET) fluorophore reporter pair within the antibody-switch, we can measure conformational changes in the switch through its fluorescence and thereby continuously measure changing target concentrations. We have validated our approach by engineering an antibody-switch that responds to the steroid digoxigenin (DIG). This antibody-switch achieved FRET-based measurement of changing concentrations across a wide dynamic range spanning ~100 nM to 1 mM, with ~5-min temporal resolution and high sensitivity even in undiluted plasma. To illustrate the generalizability of this approach, we also engineered an antibody-switch for cortisol, which exhibits similarly robust performance. By tuning the identity of the bait molecule to a cortisol analog with lower antibody affinity, we were able to further improve antibody-switch sensitivity by 100-fold. Last, we incorporated our cortisol antibody-switch into an optical fiber biosensor design. We demonstrate continuous cortisol sensing in buffer, with the ability to track fluctuating cortisol concentrations spanning the nanomolar to micromolar range with ~5-min temporal resolution for >3 hours. These sensors can reproducibly resolve cortisol concentrations across the physiological range of 10 nM to 1 μM in a buffer and can detect 100 nM changes in cortisol concentration directly in whole human blood with no sample preparation. We believe that this modular design strategy should be broadly generalizable to many existing antibodies, thereby accelerating the proliferation of continuous biosensors for new targets.

## RESULTS

### Design of an antibody-based molecular switch

In the antibody-switch design, an IgG antibody is engineered into a molecular switch that can achieve continuous biosensing of its cognate antigen with no sample preparation required. We use a DNA scaffold to link the antibody to a bait molecule—an analog of its antigen that competes with the binding of free antigen molecules present in the sample (Fig. 1A). Switching occurs when the free antigen displaces the bound bait or vice versa, leading to a conformational change in the DNA scaffold linking the bait and antibody. Target-dependent switching is quantified with high specificity through FRET-based fluorescent measurements derived from donor fluorophores on the surface of the antibody and an acceptor fluorophore incorporated within the DNA scaffold adjacent to the bait, such that the distance between donor-acceptor dye pairs increases when the antibody-switch opens in response to target binding (Fig. 1B). This target-dependent switching is described by a three-state competitive switching equilibrium (Supplementary Discussion 1). In the absence of target, the linked bait molecule binds the antibody through an intramolecular reaction ($K_D^{bait}$). When the target is present, competition between this intramolecular reaction and antibody-target binding ($K_D^{target}$) leads to switching of the construct from the closed (high FRET ratio) to the target bound (low FRET ratio) state. Both the bait and target can dissociate from the antibody after binding, such that the construct achieves reversible switching and signaling.

Although the affinity of the chosen antibody is fixed, we can tune the strength of the intramolecular reaction to control the overall sensitivity of our switch (*25*). If the bait molecule is identical to the target antigen, then intramolecular bait binding will be strong (low $K_D^{bait}$), shifting the equilibrium toward the closed state and resulting in low target sensitivity. Low sensitivity here is defined by a high median effective concentration ($EC_{50}$), which describes the free target concentration at which a half-maximal FRET switching response occurs. In contrast, a mismatched bait molecule with a higher $K_D^{bait}$ leads to weaker competition and a more target-sensitive switch (low $EC_{50}$). However, if antibody-bait binding is too weak, intramolecular binding will not occur, leading to high background from a large proportion of switches in the open but nontarget-bound state and thus a poor signal-to-noise ratio. It is also critical to ensure that the bait and free target binding are fully competitive, such that displacement of the bait is guaranteed upon target binding. This means that careful selection of the bait antigen is needed to balance strong FRET signal and sensitivity to low target concentrations. Critically, the modular antibody-switch design can be applied to different small-molecule targets by substituting the antibody-bait pair while maintaining a consistent DNA scaffold geometry and switch assembly process, as described in detail below.

### Synthesis and validation of a DIG-sensing antibody-switch

As an initial proof of concept, we developed an antibody-switch that recognizes DIG, a plant-derived steroid molecule. We first synthesized our DIG-DNA conjugate by covalently coupling DIG to the 5′ end of a 20–nucleotide (nt) single-stranded bait-DNA oligonucleotide modified with a Cy5 acceptor dye molecule 10 nt from its 5′ end (Fig. 2A; see table S1 for all DNA sequences used in this work). The selection of DIG as both the target and the bait molecule should yield a switch exhibiting strong binding between the DIG-DNA and free target (low $K_D^{bait}$) at the expense of lower switch sensitivity (high $EC_{50}$).

To quantify DIG-DNA/antibody affinity, we incubated magnetic beads coated with candidate antibodies with varying concentrations of free (not antibody conjugated) DIG-DNA, washed, and then analyzed the beads via flow cytometry to quantify the bound fraction of DIG-DNA. Because the steric impact of DNA conjugation on DIG-antibody binding is hard to predict, we tested two different antibodies—one polyclonal and one monoclonal—to ensure that this conjugation did not disrupt the competitive binding needed for proper antibody-switch function. We found that the polyclonal antibody (pAb) exhibited superior properties for constructing an antibody-switch, binding to DIG-DNA with a $K_D^{bait}$ of 5.6 nM [95% confidence interval (CI) = 4.8 to 6.4 nM], indicating that the attachment of DNA did not markedly disrupt the antibody-binding interface (Fig. 2B). We next incubated pAb-coated beads with a fixed concentration of DIG-DNA and varying concentrations of free target and measured the bound fraction of DIG-DNA that was not displaced by free DIG. Notably, free DIG robustly outcompeted DIG-DNA; with 10 nM DIG-DNA, a DIG concentration of 5.8 nM (95% CI = 5.4 to 6.2 nM) was sufficient to displace half of the bound DIG-DNA, indicating that free DIG exhibited slightly stronger antibody binding than DIG-DNA (Fig. 2C). In contrast, when we performed the same analysis with the monoclonal antibody, DIG-DNA exhibited weaker affinity, with a $K_D^{bait}$ of 91 nM (95% CI = 56 to 148 nM) and poor competitive displacement by the free target: >5 μM free DIG was required to achieve 50% DIG-DNA displacement with 10 nM DIG-DNA (fig. S1). This poorer performance was likely due

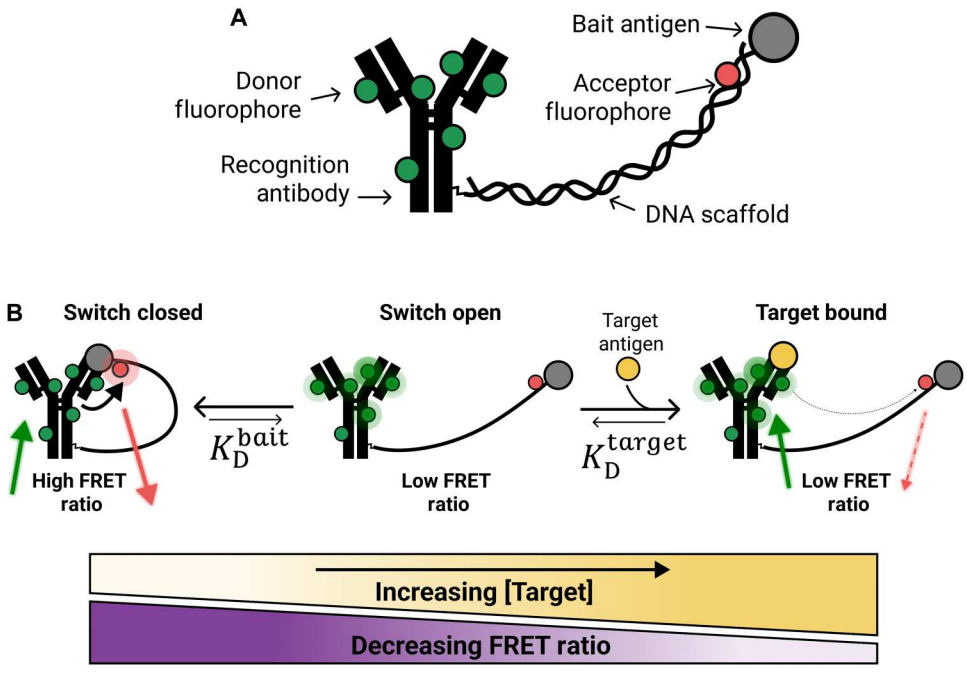


**Fig. 1. The antibody-switch construct.** (**A**) We adapt an antibody into a molecular switch by tethering it to a bait molecule through a DNA scaffold. Fluorescent quantification of changing target analyte concentrations is achieved by incorporating FRET donor and acceptor fluorophores on the antibody surface and within the DNA scaffold, respectively. (**B**) Molecular switch operates through a three-state competitive equilibrium, where increased target concentrations shift the equilibrium toward the target-bound (right) and away from the closed state (left). This equilibrium depends on the target-binding affinity of the antibody ($K_D^{target}$),but target sensitivity can also be tuned by varying the strength of intramolecular bait binding ($K_D^{bait}$). The switch exhibits a decreased FRET ratio upon target binding as the distance between the donor and acceptor fluorophores is increased in the open and bound states compared to the closed state.

to steric interference of the DNA within the DIG-DNA conjugate with the monoclonal antibody's capacity to recognize DIG in solution, and we therefore selected pAb for subsequent experiments.

We subsequently synthesized the complete antibody-switch construct (Fig. 2D). Starting from unmodified pAb **1**, we site-specifically modified the glycans on the antibody Fc domain and then conjugated these sites with a 40-nt scaffold-DNA **2** that bears a biotin moiety 6 nt from the antibody conjugation site for purposes of surface immobilization. This site-specific conjugation ensures consistency in terms of the antibody-switch geometry, which, in turn, dictates intramolecular competition and thus switching function. Any unconjugated scaffold-DNA was then removed by size exclusion purification of the antibody-DNA conjugate. Using SDS–polyacrylamide gel electrophoresis (SDS-PAGE), we determined that the resulting successfully formed antibody-DNA conjugates **3** exhibit exactly 1 DNA molecule per Fc domain, as intended (fig. S2). This antibody conjugation reaction has an efficiency of approximately 50% when measured by SDS-PAGE, as approximately 25% of heavy chains become DNA labeled. Next, we coupled the DIG-DNA complex to the antibody-DNA conjugate using enzymatic ligation. We first hybridized DIG-DNA with a partially complementary scaffold-complement sequence, where the overhang is complementary to the pAb-coupled scaffold-DNA sequence **4**. This assembly then forms the splinted 60-bp DNA scaffold for the antibody-switch, with a nick between the DIG-DNA strand and the scaffold-DNA strand **5**. Incubation with T4 ligase subsequently closes this nick **6** (fig. S3). The 60-bp scaffold length was selected as it gives a scaffold length (~20 nm) on the same order as the length and width of our immunoglobulin G (IgG) antibodies (~10 to 15 nm) while leaving sufficient distance between the acceptor dye and antibody to allow decreased FRET upon switch opening. Donor fluorophores (Alexa Fluor 546) were then incorporated by modifying the antibody's exposed lysine residues **7**. The complete switch can then be site-specifically functionalized onto a streptavidin-bearing biosensor surface via biotin-streptavidin interaction, which is reinforced by adding a BS3 amine-to-amine crosslinker to achieve covalent surface attachment **8**. Critically, this synthesis process ensures, through purification of the antibody-DNA conjugate and the high efficiency of ligation, that only fully assembled antibody-switch constructs contain the biotin moiety required for surface immobilization. This modular assembly process also allows us to substitute different bait molecules, DNA scaffolds, or antibody candidates to modify switch function.

We confirmed that our antibody-switch undergoes target-responsive FRET switching by immobilizing the switches onto streptavidin-coated magnetic beads and then incubating the beads for 1 hour with various concentrations of DIG in a buffer that was selected to match ionic concentrations in blood and interstitial fluid (ISF) [1× phosphate-buffered saline (PBS) with 1 mM $MgCl_2$ and 4 mM KCl]. We measured the fluorescent response via flow cytometry immediately afterward. As expected, the FRET ratio decreased as we introduced increasing DIG concentrations (Fig. 2E and fig. S4A). We fitted the FRET response to a Hill binding model and determined that the sensor responds with a Hill coefficient ($n$) of 0.51 (95% CI = 0.44 to 0.59) and an $EC_{50}$ of 64 μM (95% CI = 35 to 93 μM). The switch responded to changes in DIG concentration

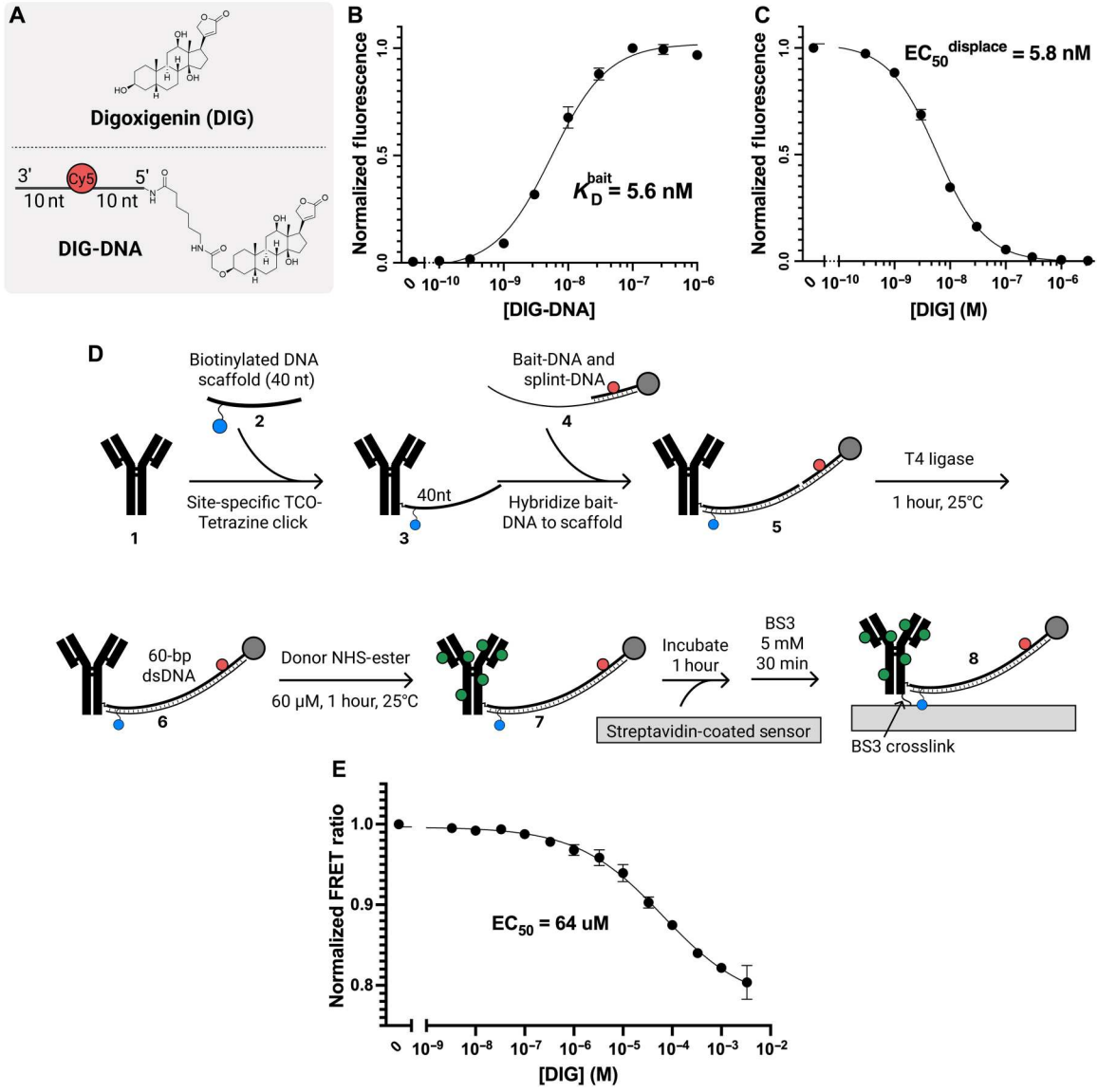


**Fig. 2. Engineering a DIG-responsive antibody-switch.** (**A**) Our DIG-DNA construct incorporates a DIG bait moiety and a Cy5 fluorescent reporter into a 20-nt DNA scaffold. (**B**) We used flow cytometry to characterize the $K_D^{bait}$ of DIG-DNA binding to a polyclonal anti-DIG antibody (pAb). (**C**) Competitive binding assays quantifying the disruption of DIG-DNA/pAb antibody pair binding by free DIG in solution suggest that the molecular competition from DIG-DNA can be used to quantify target binding. We used 10 nM DIG-DNA for all measurements in this plot. (**D**) Multistep antibody-switch synthesis process leverages site-specific antibody-DNA conjugation followed by splinted ligation to assemble a complete switch with controlled stoichiometry and a site-specific biotin handle for immobilization onto biosensor surfaces. dsDNA, double-stranded DNA. (**E**) When assembled antibody-switches are assembled on magnetic beads and measured using flow cytometry, the antibody-switch FRET signaling response spans a broad dynamic range of DIG concentrations. All data points and error bars represent the mean and SD of three replicates, respectively.

spanning a greater than 10,000-fold dynamic range, with an upper bound in the low-millimolar range and a limit of detection (LOD) of 68 nM.

## Specific, rapid, and reversible antibody-switch biosensing

We next assessed our antibody-switch's suitability for continuous biosensing in complex biofluids, where nonspecific binding by interferents poses a major challenge. We assembled antibody-switch–coated beads as described above and then tested their specificity by challenging them with DIG doped into the protein-rich environment of undiluted chicken plasma and then measuring their FRET response via flow cytometry. Before measurement, plasma samples were filtered with a 0.45 µM syringe filter to remove large particulates that interfere with flow cytometry while preserving the complete protein, small molecule, and fluid content of the plasma. The switch response in undiluted plasma was virtually identical to that in buffer, with an identical LOD of 68 nM and a largely unchanged dynamic range, where $EC_{50}$ = 87 µM (95% CI = 15 to 160 µM) and $n$ = 0.43 (Fig. 3A and fig. S4B).

The ability to sense changes in target concentration rapidly and reversibly is also crucial for continuous sensors, and we hypothesized that our linked, intramolecular design would enable rapid

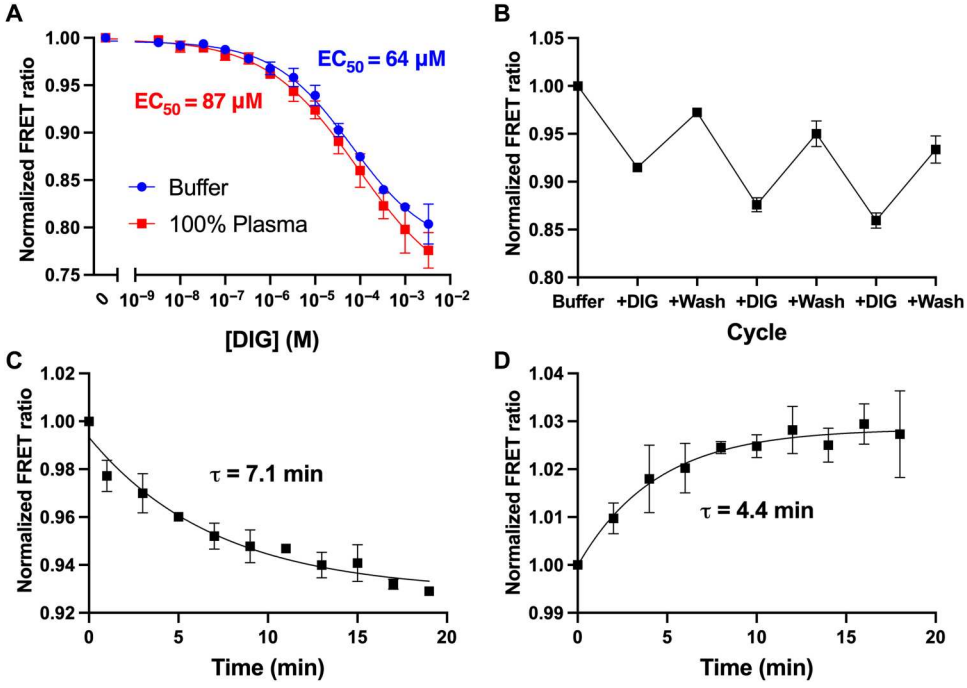


**Fig. 3. Assessing suitability of the DIG antibody-switch for continuous sensing in complex media.** (**A**) Our antibody-switch achieved essentially identical DIG-responsive FRET sensing performance in both buffer and undiluted chicken plasma when immobilized on magnetic beads and measured using flow cytometry. (**B**) Reversible binding and signaling over multiple 30-min cycles of target addition and removal indicates that our antibody-switch is suitable for repeated or continuous measurements. We observed a rapid kinetic response from our antibody-switch, with an (**C**) association time constant of 7.1 min (95% CI = 3.4 to 8.0 min) and (**D**) a dissociation time constant of 4.4 min (95% CI = 2.8 to 7.5 min). All data points and error bars represent the mean and SD of three replicates, respectively.

switching between open and closed states over many cycles of changing target concentrations. We repeatedly exposed our bead-immobilized antibody-switches to high concentrations of DIG (1 mM) in a buffer for 30 min, followed by 30-min incubations in target-free buffer. We observed reversible and repeatable FRET switching over the course of a 3-hour experiment involving three cycles of target addition and washout (Fig. 3B). We observed a small degree of FRET ratio decrease over each cycle, and we hypothesized that this may be due to degradation of the bead surface or residual DIG that remains after wash cycles. Despite this degradation, the reversible response demonstrated over many cycles indicates that the switch mechanism is reversible and could be suitable for achieving continuous sensing in surface-based biosensor formats that are better optimized for continuous sensing.

We also measured the antibody-switch's FRET response kinetics upon DIG addition and washing with buffer. We observed rapid changes in FRET ratio in terms of both target binding ($\tau_{on}$ = 7.1 min; Fig. 3C) and dissociation ($\tau_{off}$ = 4.4 min; Fig. 3D). This indicates suitable performance for collecting continuous measurements with a temporal resolution of ~5 min and potentially faster if sensor response is characterized with a pre-equilibrium approach (*26*). The roughly symmetric kinetic response to increasing or decreasing target concentrations is consistent with our competitive binding model, where both on- and off-switching events require the slow dissociation of either the free target or the bait (Supplementary Discussion 1).

## Engineering a cortisol-responsive antibody-switch with enhanced sensitivity using a mismatched bait design

As described above, our antibody-switch design can be readily tailored for different target biomolecules by simply substituting the antibody-bait pair, and we demonstrated this capability by engineering an antibody-switch for cortisol. Cortisol is an important stress hormone that affects nearly every organ system in the body, playing a critical role in stress, metabolism, and inflammation (*27*, *28*). We hypothesized that by using a cortisol analog as a bait molecule, we could tune the intramolecular competition within our switch—and thus its affinity for free cortisol—to achieve sensitive detection over clinically relevant cortisol concentrations, which span approximately 1 nM to 1 μM in the blood and ISF (*29*). We chose a cortisol-binding monoclonal antibody and then screened antibody binding and competitive displacement for bait-DNA conjugates incorporating either cortisol or corticosterone (a cortisol analog with a missing hydroxyl group near position 21, where antibody recognition occurs) as the bait molecule (Fig. 4A). The bait-DNA incorporating cortisol (Cort-DNA) exhibited a low $K_D^{bait}$ of 1.8 nM (95% CI = 1.6 to 2.0 nM; Fig. 4B, blue) and competed strongly with free cortisol, with 41 nM cortisol (95% CI = 30 to 56 nM) required to achieve 50% displacement of bound Cort-DNA in the presence of 10 nM bait-DNA (Fig. 4C, blue). In contrast, the corticosterone bait-DNA (CSO-DNA) exhibited a higher $K_D^{bait}$ of 4.7 nM (95% CI = 3.7 to 6.0 nM; Fig. 4B, green) and approximately sevenfold weaker competition with free cortisol, with only 5.8 nM (95% CI = 5.3 to 6.3 nM) free cortisol required to achieve equivalent displacement of 10 nM CSO-DNA (Fig. 4C, green).

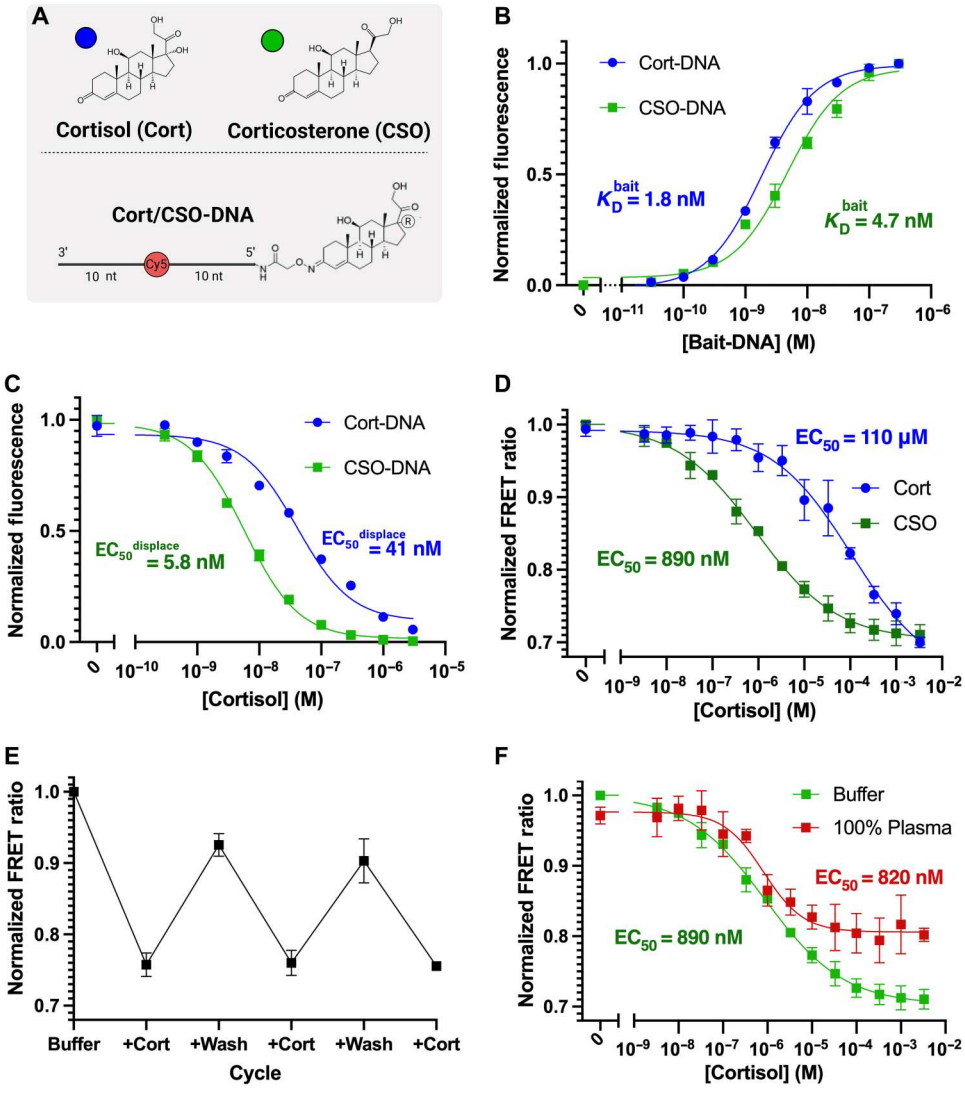


**Fig. 4. Cortisol antibody-switch engineering.** (**A**) Our cortisol antibody-switch incorporated either cortisol (Cort-DNA) or corticosterone (CSO-DNA) as the bait molecule at the end of the 20-nt DNA scaffold. (**B**) Monoclonal anti-cortisol binding to bait-DNA conjugates. When CSO-DNA is used in place of Cort-DNA, we measured a higher $K_D^{bait}$ in bead-based antibody binding assays, indicating that corticosterone may act as a weaker competitor molecule. (**C**) Competitive binding assays of bait-DNA conjugates against free cortisol further demonstrate that CSO-DNA acts as a weaker competitor than Cort-DNA. All experiments were conducted with 10 nM bait-DNA. (**D**) Cortisol-dependent FRET responses of antibody-switches incorporating Cort-DNA or CSO-DNA in a buffer. Both switches respond to a wide dynamic range of cortisol concentrations, but the CSO-DNA construct achieves higher sensitivity due to weaker intramolecular competition. (**E**) CSO-DNA antibody-switch exhibits reversible binding over multiple cycles of target addition and washing. (**F**) This switch also maintains robust cortisol sensing in undiluted chicken plasma. All data points and error bars represent the mean and SD of three replicates, respectively.

We followed the modular synthesis process described above to construct antibody-switches that combine XM210 with either Cort-DNA or CSO-DNA (figs. S2 and 3B) and then immobilized these onto streptavidin beads. Both switches exhibited decreasing FRET ratios at increasing target concentrations, indicating successful assembly of cortisol-responsive molecular switches (Fig. 4D and fig. S5, A and B). The Cort-DNA switch achieved modest cortisol sensitivity, spanning from an LOD of 340 nM up to a maximum tested concentration of 3.3 mM. In comparison, the mismatched CSO-DNA bait enhanced antibody-switch sensitivity by ~100-fold, with an LOD of 3.3 nM and an upper limit of quantification of 95 µM. This means that the CSO-DNA switch is likely to be better suited for monitoring clinically relevant cortisol concentrations. These results highlight how the selection of alternative analogs as bait can enable further optimization of sensor performance for a given analyte.

We performed additional experiments to assess how changes in the scaffold length affect intramolecular competition and whether this feature can be tuned to further optimize switch sensitivity. We adapted our ligation-based scaffold assembly to accommodate additional DNA tile strands, extending the scaffold length from 60–base pair (bp) to 120- and 180-bp using the CSO-DNA bait (fig. S6A). We tested the cortisol response of these switches in the same bead-based assay and observed minimal effect of scaffold

length on switch sensitivity (fig. S6B). We hypothesized that this can be attributed to the fact that we were performing sensing using a surface that is densely coated with switches, such that increasing the scaffold length allows a given bait molecule to compete less strongly with its own linked antibody but more strongly with neighboring antibodies and thus does not produce a net change in competitive switching behavior. We therefore continued to use the 60-bp scaffold design for our remaining experiments as it allows for the simplest switch assembly. However, we note that for other larger bait molecules, it may be useful to optimize the scaffold geometry using this modular ligation approach.

Similar to the DIG-responsive antibody-switch, the CSO-DNA switch exhibited robust reversibility and specificity in complex biofluids. When exposed to multiple 30-min cycles of 1 mM cortisol and washout with target-free buffer, the bead-immobilized CSO-DNA antibody-switches exhibited stable and reversible on-and-off switching (Fig. 4E). We also tested our antibody-switch in chicken plasma, which was chosen as it shares a similar level of protein content to human plasma but contains corticosterone rather than cortisol, thus reducing cross-reactivity with endogenous species (*30*). The cortisol-responsive switch maintained its switching behavior and ability to sense spiked in cortisol with good sensitivity in undiluted plasma, with an LOD of 140 nM (Fig. 4F and fig. 5C). This is lower than the sensitivity we observed in a buffer, most likely due to high levels of cortisol binding to plasma proteins such as albumin and transcortin, which may attenuate the free (non-protein–bound) levels to only 5 to 25% of the spiked-in cortisol concentration (*29*, *31*). However, because the free fraction of cortisol is the only bioactive fraction, this may not impede our switch's applicability for diagnostic purposes (*32*). We also observed a decreased FRET response amplitude in plasma compared to buffer. This may be attributable to switch binding to endogenous corticosterone present in chicken plasma or opening of the switch in response to plasma proteins binding to the bait molecule. Either of these effects would decrease the FRET ratio in the absence of cortisol, leading to decreased overall signal amplitude. Despite these complicating factors, these results demonstrate the value of the antibody-switch design as a tool for achieving continuous biosensing in complex matrices.

We further tested the specificity of our CSO-DNA antibody-switch against structurally similar small molecules that may be present in biofluid samples. We tested DIG as well as corticosterone, prednisolone, and progesterone—lower abundance hormones that share biosynthetic pathways with cortisol—and compared the switch cross-reactivity to the intrinsic cross-reactivity exhibited by the constituent XM210 antibody in unlinked competition assays. We found that the antibody exhibited partial cross-reactivity with corticosterone and prednisolone, owing to their high structural similarity to cortisol, but has no cross-reactivity to DIG or progesterone (fig. S7A). The cross-reactivity of our antibody-switch (fig. S7B) closely matched that of the antibody, confirming that the antibody dictates the overall performance of the switch. The observed corticosterone cross-reactivity also supports the hypothesis that endogenous corticosterone contributes to the decreased signal amplitude observed in plasma for the CSO-DNA switch. This similarity in cross-reactivity profiles demonstrates that the specificity of the switch is dependent on the properties of the starting antibody and that the switch design does not introduce any additional cross-reactivity.

### Continuous cortisol biosensing with antibody-switches

Last, we assessed the continuous sensing performance of our antibody-switch when incorporated with an optical fiber-based biosensor described previously by our group (*33*). This system comprises a tapered optical fiber sensor functionalized with a monolayer of antibody-switches assembled onto the fiber tip surface via streptavidin-biotin immobilization (Fig. 5A, inset). To assemble this sensor, tapered optical fibers were coated in a polyethylene glycol (PEG) passivation layer bearing a limited number of biotin end groups (1% of the monolayer). These biotin groups were then coupled to the biotinylated antibody-switches via streptavidin molecules. The tapered profile of the fiber optic tip leads to the formation of an evanescent field of light excitation that is confined close to the sensor surface, only penetrating a few hundred nanometers into solution. This evanescent sensing strategy enables selective excitation of donor dyes within the antibody-switch without eliciting meaningful background from unbound molecules in the sample. It also enables efficient collection of emitted light from both donor and acceptor dyes for FRET ratio measurements. This optical fiber sensor is placed within a ~ 50 μl of sample chamber that allows us to flow samples across the sensor surface (Fig. 5A). An optical reader couples laser excitation light into the optical fiber sensor and then collects and measures the emitted light from antibody-switches immobilized onto the sensor surface. This enables continuous measurement of the sensor FRET response as target concentrations change.

For continuous sensing experiments, we substituted the Cy5 acceptor dye with ATTO643, which exhibits better photobleaching resistance. To allow orthogonal modification of the bait-DNA with both our bait molecule and this enhanced dye, we used copper-free click chemistry to attach ATTO643 to an alkyne modification situated four bases away from the bait molecule (see "bait-DNA-Alkyne4" in table S1). We moved the dye molecule closer to the bait in this design in an effort to increase FRET in the closed state and thus increase the FRET ratio change upon switching. Substituting the acceptor dye did not produce any substantial changes in the switching affinity of the Cort-DNA-Alkyne4 or CSO-DNA-Alkyne4 antibody-switches, and moving the dye to a position 4 nt from the bait increased the binding-induced FRET response in the CSO-DNA-Alkyne4 switch (fig. S8, A and B). In addition, ATTO643 exhibited ~20-fold slower photobleaching when exposed to continuous laser illumination compared to Cy5 (fig. S8C). To further increase the long-term fluorescent stability of our sensor, we used intermittent laser excitation, acquiring measurements every 30 s. Because even slow photobleaching effects accumulate over time, data were corrected by first acquiring a photobleaching calibration measurement over 15 min in the absence of target and then subtracting this calibrated photobleaching slope over the duration of measurement (fig. S9).

We demonstrated the performance of our CSO-DNA-Alkyne4 antibody-switch–coupled fiber optic sensor over a series of stepwise cortisol concentration changes. We injected buffer spiked with varying cortisol concentrations into the measurement chamber to vary the free target concentration seen by the sensor at regular intervals and then allowed the sensor to equilibrate in the solution without flow while continuously measuring the FRET response. Figure 5B shows the FRET response over >3 hours of continuous measurement, plotted as the inverse of the FRET ratio change, such that increased concentrations are represented by increasing

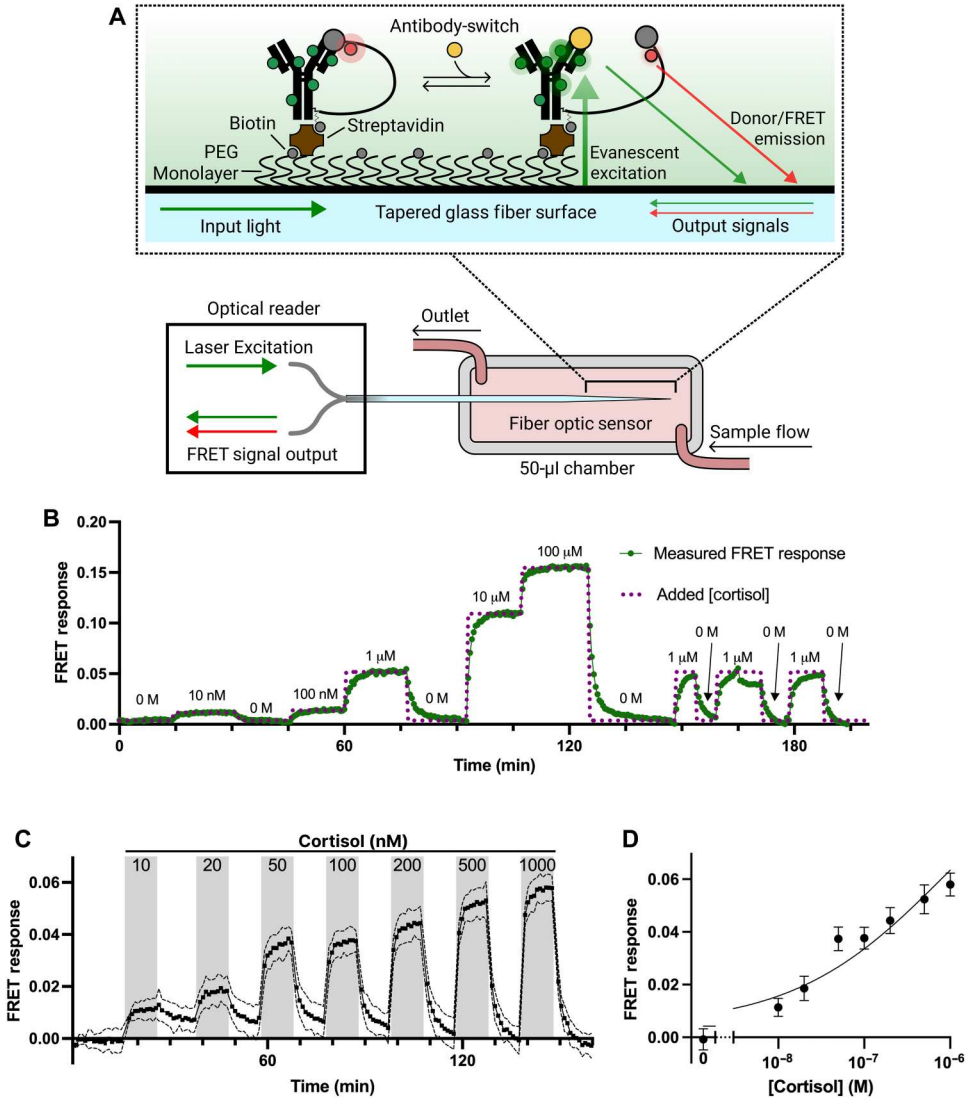


**Fig. 5. Continuous cortisol sensing with antibody-switches coupled to a fiber optic sensor.** (**A**) Diagram of the setup for our tapered fiber optic sensor. The fiber tip is functionalized with antibody-switches via biotin-streptavidin immobilization onto a PEG monolayer. Laser light travels to the fiber tip and excites antibody-switch donor fluorophores within the evanescent field generated along the tapered portion of the fiber. The resulting donor and FRET emission is then coupled back to measurement instrumentation through the fiber. The measurements themselves are performed within a 50-µl flow chamber. (**B**) Continuous FRET measurement of changing cortisol concentrations in buffer over the course of a 3+-hour experiment. Buffer spiked with various concentrations of cortisol (purple dotted curve) was injected into the chamber at 5- to 15-min intervals, and the antibody-switch FRET response was measured continuously. The presented FRET response data are corrected for the effects of photobleaching and plotted as the absolute value of the FRET ratio change from the baseline, so that increased concentrations lead to increased rather than decreased signals. (**C**) Continuous measurement of cortisol within the physiological concentration range of 10 nM to 1 µM using fiber optic sensors. Solid and dashed lines, respectively, represent the mean and SD of $n = 3$ independently fabricated and functionalized sensors. (**D**) Steady-state FRET response values extracted from continuous measurements show the concentration-dependent sensor response. Data points and error bars, respectively, represent the mean and SD of the last three data points upon saturation from $n = 3$ fiber optic sensors.

rather than decreasing signals. As in our bead-based assays, the switch was sensitive to sharp increases and decreases in cortisol concentration across a ~10,000-fold dynamic range, detecting spikes as low as 10 nM and as high as 100 µM. Over the course of this measurement, the sensor responded rapidly to rising and falling cortisol concentrations, achieving equilibration in <5 min at all measured concentrations (fig. S10). Critically, the sensor maintained a stable baseline over the course of many cycles of increasing and decreasing target concentration.

We then investigated the reproducibility and performance of our sensors at physiological cortisol concentrations in more detail by testing three independently fabricated and functionalized antibody-switch fiber sensors in parallel. Because the geometry of the fiber optic tapers used for sensing varies slightly from fiber to fiber, the FRET signal amplitude also varies between fibers and thus requires a simple calibration method to ensure repeatable results. We performed single time point calibration, normalizing measured FRET ratios based on the first FRET ratio measurement

in target-free buffer, and then applied the photobleaching correction described above. This simple single time point calibration approach is similar to the factory calibration approaches used to improve reproducibility in commercial CGMs (*34*).

We then tested these sensors' continuous-mode performance in buffer at cortisol concentrations spanning 10 nM to 1 μM to simulate low and high physiological concentrations in human ISF or blood (Fig. 5C). We observed reversible and rapid sensing across this range. We observed that the sensors approached their steady-state values within 10 min of each step change in cortisol concentration. The sensors also returned to a stable baseline upon washing with buffer throughout the >2.5-hour measurement period. To assess sensor resolution at these concentrations, we extracted the steady-state FRET response values from our continuous measurements, obtaining a sensor response curve (Fig. 5D). This curve indicated that our calibrated sensor is consistently capable of discriminating low cortisol concentrations (10 nM) from higher (≥100 nM) concentrations of cortisol. We subsequently calculated an LOD of 1.2 nM, which falls below our lowest demonstrated measurement of 10 nM and is consistent with the LOD we obtained with our bead-based measurements.

As a final proof of concept, we tested our antibody-switch biosensor's performance in sensing physiological cortisol concentrations directly in 99% human whole blood with no sample preparation. We measured the response of three independently fabricated sensors to repeated cycles of cortisol increase and decrease in healthy human donor blood over a 45-min measurement (Fig. 6). Beginning from a baseline measurement in buffer, the sensor exhibited a substantial change in signal when exposed to human blood due to both the endogenous cortisol present in the blood sample and changes in optical properties due to blood's absorbance. The sensors were then exposed to the same donor blood spiked with an additional 100 nM cortisol to mimic a physiological increase from the endogenous baseline, and we repeated this exposure to unspiked and spiked blood for multiple cycles. The sensor response captured these 100 nM increases and decreases in cortisol, and the response to each concentration change was resolved within 5 min. It should be noted that these blood-based measurements suffered from issues associated with clotting and biofouling, resulting in inconsistent sensor response across cycles as well as drift and signal degradation over time. Nevertheless, the ability to continuously detect physiological cortisol spikes in unmodified whole human blood is an important advance, laying the groundwork for future efforts to develop more robust performance in undiluted biofluids.

## DISCUSSION

The antibody-switch design provides a way to engineer existing antibodies into target-responsive molecular switches capable of real-time continuous biosensing. Our constructs link an antibody to a bait molecule through a DNA scaffold, enabling competitive binding with the free target that gives rise to conformational switching events that can be detected via FRET. These switches exhibit desirable properties for biosensing, including a broad (~10,000-fold) dynamic range, rapid kinetics, reversibility, and the ability to sense targets directly in undiluted biofluids. The antibody-switch design is also modular and generalizable, such that it can be tailored to a broad range of targets simply by exchanging the antibody and bait molecule, as we have demonstrated in experiments using antibody-switches for DIG and cortisol. This modularity also allowed us to tune the sensitivity of our cortisol-responsive antibody-switch by replacing the cortisol bait with a mismatched corticosterone bait, which enhanced the switch's target affinity ~100-fold. By integrating our switch into a miniaturized fiber optic sensor probe, we were able to achieve continuous cortisol sensing across a concentration range of 10 nM to 100 μM with temporal resolution of ~5 min and stability over >3 hours in buffer. We further demonstrated that these sensors can reproducibly resolve cortisol concentrations across the physiological range of 10 nM to 1 μM in a buffer and that these sensors repeatedly detect 100 nM changes in cortisol concentration in whole human blood with no sample preparation. These preliminary results suggest that antibody-switches may offer a



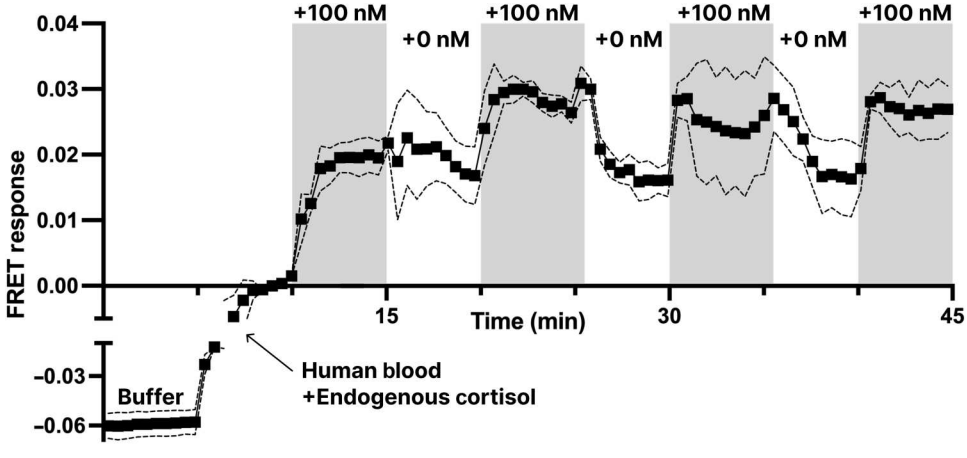


**Fig. 6. Continuous antibody-switch biosensing in 99% whole human blood.** The fiber optic cortisol sensor was challenged with alternating 5-min cycles of healthy human donor blood containing endogenous cortisol concentrations or the same blood spiked with 100 nM cortisol to simulate a physiologically relevant increase from the baseline. The sensor was first prepared in a buffer and then allowed to equilibrate in unspiked blood before testing the sensor response to alternating cycles of unspiked and spiked blood (indicated by arrows on the plot). Solid and dashed lines, respectively, represent the mean and SD of measurements from $n = 3$ independently prepared sensors.

general and robust method for developing switch-based continuous biosensors.

We believe that our antibody-switch design represents a valuable addition to the rapidly growing toolbox of protein-based biosensors. For example, Easley and coworkers have made use of competitive binding of solution-phase antibodies to enable small-molecule sensing using antigen-modified DNA structures on electrochemical sensors (*35*–*37*). However, because these sensors rely on the introduction of free antibody into solution to achieve competitive binding, they are unsuitable for continuous sensing. Kang *et al.* (*38*) have demonstrated the use of redox-modified protein-based molecular switches for reagent-free sensing of specific protein binding partners, demonstrating tunable signal gain and high sensitivity in diluted plasma, but it is unclear how this approach could be adapted to sensing small molecules that lack naturally occurring, structure-switching protein receptors. In another notable recent advance, the molecular pendulum approach developed by Das *et al.* (*23*) offers an antibody-based approach to sense protein targets in biofluids. This approach achieves high-sensitivity protein detection and is compatible with a range of biofluids and can readily be generalized to a wide range of protein targets by substituting the target-binding antibody. The key limitation of this approach is that it may be difficult to apply to small-molecule targets because the sensing mechanism relies on substantial changes in pendulum dynamics upon target binding, which typically requires higher–molecular weight analytes. Our antibody-switch complements these various molecular detection technologies by enabling the continuous sensing of small molecules at time scales and concentrations that are appropriate and physiologically relevant for the clinical analysis of small-molecule biomarkers such as cortisol. Other small-molecule sensing schemes have emerged recently that leverage competitive binding to achieve continuous sensing by tracking particle mobilities (*39*, *40*), but we believe that our FRET-based readout mechanism and sensor design are more compatible with the miniaturized sensor probe designs required for biomedical applications such as wearable or implantable sensors.

Future iterations of this system could enable continuous sensing of a broader range of targets, including peptides and even small proteins. The scaffold length can readily be modified during antibody-switch assembly and thus should accommodate the inclusion of the larger peptide- or protein-based bait molecules needed to sense these targets. These targets may require increased sensitivity, and mismatched bait designs that weaken competitive binding beyond what was demonstrated with corticosterone may yield sensors that are capable of detecting analytes in the range of 10 pM to 1 nM. However, at these low concentrations, the antibody′s intrinsic properties will impose fundamental limitations on sensitivity. The lowest achievable $EC_{50}$ in this competitive switch design is determined by the antibody′s affinity, and few antibodies exhibit affinities below the 10 pM range. Furthermore, the temporal resolution of continuous measurement is limited by the antibody off-rate. Because this off-rate typically decreases with higher affinity, low-abundance targets may not be suitable for sensing at single-minute resolution. However, careful optimization of the sensor by screening for faster off-rate antibodies and using emerging computational approaches that enhance the temporal resolution of measurements made with slow-responding receptors could facilitate the development of continuous sensing applications for low-abundance analytes (*26*, *41*). We have also observed that biofouling remains a substantial challenge to stable sensing in whole biofluids, as is the case for most biosensors. Cell and protein binding to the fiber optic probe surface contributes to noise, drift, and signal attenuation, degrading sensor performance. However, strategies for stabilizing surface-based biosensors such as membrane protection (*42*), high-performance chemical passivation strategies (*43*, *44*), or the use of nanoporous electrodes that protect receptors from proteins and cells in bulk biofluid (*45*, *46*) could greatly enhance sensor performance in in vivo settings.

Critically, our design provides a general strategy for transforming antibodies into a monolithic sensor construct that achieves target recognition, molecular switching, and fluorescent signaling with only minimal screening effort required and without any engineering of the antibody protein itself. This approach thus eliminates the need for unique proteins with intrinsic switching, high-throughput combinatorial selection assays, or case-by-case redesign of the switch structure. Hence, we believe that this antibody-switch approach has the potential to accelerate development of a diverse range of continuous biosensors for physiological monitoring and improved patient care.

## MATERIALS AND METHODS

### Reagents and materials

All oligonucleotide sequences (table S1) were purchased high-performance liquid chromatography (HPLC)–purified from Integrated DNA Technologies with various internal and terminal modifications as specified in their sequences. Cortisol monoclonal antibody (XM210) was obtained from Abcam. DIG pAb (Sheep, SKU: 11333089001) was obtained from Sigma-Aldrich, and DIG monoclonal antibody (clone no. 611621) was obtained from R&D Systems. T4 ligase and low–molecular weight DNA ladder were obtained from New England Biolabs (NEB). Methyltetrazine Dibenzocyclooctyne, TCO–*N*-hydroxysuccinimide (NHS) ester (Axial), and BTTES (3-{4-[(Bis{[1-(tert-butyl)-1H-1,2,3-triazol-4-yl]methyl}amino)methyl]-1H-1,2,3-triazol-1-yl}propane-1-sulfonic acid) were purchased from Click Chemistry Tools. ATTO643 azide was purchased from ATTO-Tech GmbH. VECTABOND reagent was purchased from Vector Laboratories. All DNA synthesis reagents—including 5′-amino-modifier C6, alkyne-modifier serinol phosphoramidites, and Glen-Pak DNA purification cartridges—were purchased from Glen Research. Biotin-PEG-SVA [molecular weight (MW) of 5000] and Methoxy poly(ethylene glycol) succinimidyl valerate (mPEG-SVA) (MW of 5000) were purchased from Laysan Bio. Amicon Ultra-0.5 size exclusion columns, DIG, DIG NHS-ester (DIG-NHS), hydrocortisone, hydrocortisone 3-(*O*-carboxymethyl)oxime, *O*-(carboxymethyl)hydroxylamine hemihydrochloride, *N*,*N*′-dimethylformamide (DMF), dimethyl sulfoxide (DMSO), sodium ascorbate, and copper (II) sulfate were purchased from Sigma-Aldrich. Cortisol-3CMO [*O*-(carboxymethyl)hydroxylamine hemihydrochloride)], 1-ethyl-3-(3-dimethylaminopropyl)carbodiimide hydrochloride (EDC), NHS, Alexa Fluor 546 NHS ester (succinimidyl ester), Dynabeads protein G, Dynabeads T1, SiteClick antibody azido modification kits, bis(sulfosuccinimidyl)suberate (BS3), tris-HCL (1 M, pH 7.5), magnesium chloride, 10× PBS (pH 7.4), adenosine 5′-triphosphate (ATP), NuPAGE sample reducing agent, NuPAGE LDS sample buffer (4×), NuPAGE 4 to 12% bis-tris mini protein gels, 20× NuPAGE MES SDS running buffer, SeeBlue prestained protein standard,

SimplyBlue SafeStain, UltraPure Tris-borate-EDTA(TBE) buffer (10×), Novex TBE-Urea Gels (10%), GelStar nucleic acid gel stain, and Tween 20 were purchased from Thermo Fisher Scientific. Heparinized heathy human donor whole blood was obtained from the Stanford Blood Center and was stored at 4°C until 30 min before measurement and used within 36 hours of collection.

### Instrumentation

Standard automated oligonucleotide solid-phase synthesis was performed on an Expedite 8909 synthesizer from Biolytic Lab Performance. DNA was quantified by ultraviolet absorbance at 260 nm with the NanoDrop 2000 spectrophotometer from Thermo Fisher Scientific. Gel electrophoresis was carried out on a 20 cm–by–20 cm vertical Hoefer 600 electrophoresis unit. Gel images were captured using a ChemiDoc MP System from Bio-Rad Laboratories. Thermal annealing of all DNA structures was conducted using an Eppendorf Mastercycler 96-well thermocycler. Flow cytometry was performed using an SH800 cell sorter from Sony Biotechnology. Mass spectrometry (MS) was performed using a microflex matrix-assisted laser desorption/ionization time-of-flight (MALDI-TOF) instrument from Bruker. Shaking was done using a ThermoMixer F1.5 from Eppendorf.

### DIG bait-DNA synthesis

DIG bait-DNA conjugates were prepared by labeling the amine in the bait-DNA sequence with DIG-NHS. DIG-NHS was dissolved in 15 mM DMF and then added to the bait-DNA in 100 mM sodium bicarbonate (pH 9) to achieve final concentrations of 82 μM DNA and 1.2 mM DIG-NHS in a 122-μl reaction volume. This mixture was incubated with rotation overnight at room temperature, then purified via ethanol precipitation, and resuspended in deionized (DI) water to ~100 μM before use. MS was used to validate DNA modification.

### Testing binding and competition for bait-DNA candidates

Pairs of target-binding antibodies and bait-DNA conjugates were screened to assess their affinity and the ability of free target to compete with their binding. All assays were performed in physiological buffer [1× PBS (pH 7.4) with 1 mM $MgCl_2$, 4 mM KCl, and 0.05% Tween 20]. The antibodies were first immobilized onto Dynabeads protein G by diluting 6 μl of stock Dynabeads (30 mg/ml) into 600 μl of 230 nM antibody in buffer. Beads were incubated for 1 hour and then washed and resuspended in 6 ml of buffer. Samples for each bait-DNA/target concentration were prepared by mixing 90 μl of antibody-coated beads with 10 μl of bait-DNA/target solution to achieve the final desired concentrations. For the bait-DNA binding assays, no target was included, and the concentration of bait-DNA varied between 0 and 3 μM. For competition assays, bait-DNA concentrations were held constant at 10 nM and free DIG concentrations (stock prepared at 100 mM in DMSO) were varied between 0 and 100 μM. To test the target specificity in these competition assays, the same density and volume of antibody-coated beads was incubated with 10 nM bait-DNA and either 1 or 100 nM cortisol, corticosterone, DIG, prednisolone, or progesterone in 0.1% DMSO. Antibody-coupled beads were incubated in these solutions for 1 hour and then resuspended in 200 μl of buffer immediately before measuring on a cell sorter to quantify Cy5 fluorescence.

### Cortisol and corticosterone bait-DNA synthesis

The Cort-DNA conjugate was prepared by coupling cortisol-3CMO to the terminal amine on the bait-DNA sequence using EDC/NHS chemistry. First, we combined 50 μl of 100 mM steroid-3CMO conjugate in 100% DMSO, 50 μl of 100 mM sulfo-NHS in 50% DMSO, and 5 μl of 100 mM EDC in 100% DMSO and then shook this mixture at 1500 rpm for 30 min at room temperature using a thermomixer. We then added 100 μl of 100 to 500 μM DNA and 40 μl of 1 M sodium bicarbonate (pH 9) and incubated this mixture for 2 hours at room temperature. The DNA was buffer-exchanged into DI water using a 3-kDa MWCO Amicon Ultra-0.5 centrifugal filter, then purified using HPLC, and validated for correct bait conjugation via MS.

CSO-DNA was synthesized by adapting a previously described protocol (*47*). A carboxyl group was conjugated onto corticosterone by combining 1.480 ml of 75 mM carboxymethoxylamine hemihydrochloride in methanol, 1.184 ml of 125 mM corticosterone in methanol, and 23.7 μl of pyridine. This solution was mixed by shaking at room temperature for 5 hours. To remove unreacted carboxymethoxylamine, the solution was dried, leaving behind a salt. This was resuspended in 1 ml of ethyl acetate and 1 ml of DI water, vortexed, and then centrifuged for 1 min at 2000*g* until the ethyl acetate and water were separated from each other. The water phase was discarded, an additional 1 ml of DI water was added, and the process was repeated for a total of three washes. After discarding the final wash, the ethyl acetate solution was dried, and the resultant solid was weighed. We recovered 61.6 mg of corticosterone with carboxyl linker. At this stage, the powder contained corticosterone with one to two carboxyl groups conjugated at different locations. The corticosterone-CMO was then conjugated onto the bait-DNA sequence using the EDC/NHS reaction described above. The resulting corticosterone-conjugated DNA was buffer-exchanged into DI water using a 3-kDa MWCO Amicon Ultra-0.5 centrifugal filter, then purified using HPLC, and validated for correct bait conjugation via MS.

### DNA-bait synthesis with ATTO643

Alkyne-bearing DNA oligos (bait-DNA-alkyne4 and bait-DNA-alkyne10) were synthesized using an Expedite 8909 DNA synthesizer at 1 μmol scale. Coupling efficiency during synthesis was monitored after removal of the DMT 5-OH protecting group. After deprotection with a 1:1 aqueous ammonium hydroxide:methyl amine (AMA) solution for 15 min at 65°C, DMT-ON purification of DNA oligos was performed using Glen-Pak DNA purification cartridges following the standard manufacturer's procedure. Before use, the purified DNA was quantified based on absorbance at 260 nm. The terminal amines of these alkyne-bearing DNA strands were then modified with cortisol or corticosterone following the same protocol as for the Cy5-containing strands. ATTO643 azide was coupled to the cortisol- or corticosterone-modified strands using copper-catalyzed azide-alkyne cycloaddition as described previously (*48*). Briefly, we prepared ~20 μM DNA and ~150 μM ATTO643 azide in 100 mM PBS (pH 7) and added premixed 500 μM BTTES ligand and 100 μM copper (II) sulfate, along with 5 mM sodium ascorbate. This mixture was incubated for 1 hour at room temperature, then purified using a 3-kDa MWCO Amicon Ultra-0.5 centrifugal filter followed by a Glen Gel-Pak 0.2 Desalting Column to exchange the labeled DNA into DI water. Last,

the ATTO643-labeled DNA was purified using HPLC and validated for correct bait and dye conjugation using MS.

### Synthesis of the antibody-switch

For this first step in the antibody-switch preparation process, ~250 μg of antibodies were modified as directed in the SiteClick antibody azido modification kit to enzymatically attach azide groups to glycosylation sites in the Fc region of the antibody, yielding a final volume of ~100 μl of 10 μM antibody. Then, 200 mM methyltetrazine DBCO in DMF was added to this ~100 μl of azide-modified antibody to achieve a final concentration of 6.7 mM methyltetrazine DBCO. This step converts the azide into a methyltetrazine group for more efficient click modification with the DNA scaffold. This mixture was incubated for 2 hours at room temperature and then purified with a 50-kDa MWCO Amicon Ultra-0.5 centrifugal filter to remove all free methyltetrazine DBCO. TCO-NHS (axial) was dissolved to 15 mM in anhydrous DMF and then added to scaffold-DNA in 100 mM sodium bicarbonate (pH 9) to achieve final concentrations of 66 μM DNA and 3.75 mM TCO-NHS. This mixture was incubated with rotation overnight at room temperature, then purified with ethanol precipitation, and resuspended in DI water to ~100 μM before use. MS was used to confirm DNA modification. The methyltetrazine-modified antibody and TCO-modified scaffold-DNA were then mixed to achieve a final DNA concentration of 40 μM (and a minimum 3:1 DNA:antibody excess) in 1× PBS. This mixture was incubated overnight at room temperature and then purified with a 50-kDa MWCO Amicon Ultra-0.5 centrifugal filter to remove any free DNA. The degree of labeling was quantified with reducing SDS-PAGE by comparing the intensity of bands from unmodified antibody heavy chains to the intensity of heavier bands formed from specific DNA conjugation to the antibody heavy chains (fig. S2, A and B). The complete removal of free DNA was assessed by denaturing DNA gel electrophoresis, noting the absence of bands corresponding to free scaffold-DNA and the formation of a heavy band corresponding to the antibody-DNA conjugate (fig. S2C). These gels were prepared by diluting either antibody-DNA or reference scaffold-DNA samples to ~400 nM in 1× TBE buffer and then mixing in a 1:1 ratio with 95% formamide-loading dye and heating to 95°C for 2 min. A ladder sample was prepared by diluting low–molecular weight DNA ladder to 1× in a 1:1 mixture with formamide loading dye and then heating to 95°C for 2 min. Each sample (4 μl) was loaded onto Novex TBE-Urea Gels (10%) and run for 40 min at 180 V in 1× TBE buffer before staining with GelStar nucleic acid gel stain for 5 min and imaging.

Splinted ligation was used to covalently attach the bait-DNA conjugate to the antibody-DNA conjugate with various scaffold lengths. To assemble the 60-bp scaffold, 3.5 μM bait-DNA was annealed with 3 μM scaffold–complement DNA in ligation buffer [50 mM tris-HCl (pH 7.5), 10 mM $MgCl_2$, and 1 mM ATP] by preparing a 17-μl reaction volume, heating the mixture to 95°C, and then cooling to 4°C for 30 min. To assemble the 120-bp scaffold, the same procedure was performed, but with the reaction volume containing 3 μM scaf120_c2 DNA, 3.3 μM scaf120_ligate DNA, 3.5 μM scaf120_c1 DNA, and 3.75 μM bait-DNA. To assemble the 180-bp scaffold, the same procedure was performed but with the reaction volume containing 3 μM scaffold_c2 DNA, 3.3 μM scaf120_ligate DNA, 3.5 μM scaf180_c1 DNA, 3.75 μM scaf180_ligate DNA, 4.1 μM scaf180_c0 DNA, and 4.3 μM bait-DNA. Then, 40 μl of ~500 nM antibody-DNA conjugate was mixed with the entire annealed mixture in ligation buffer and incubated for 1 hour at room temperature to allow for hybridization. This mixture (56.3 μl) was then combined with 13.5 μl of ligation solution, comprising 2700 U of T4 ligase (6.75 μl of 400,000 U/ml) in ligation buffer, and incubated for 1 hour at room temperature to achieve complete ligation into a covalently linked antibody-switch molecule. The success of this ligation was monitored using reducing SDS-PAGE. For the SDS-PAGE analyses mentioned here and above, these products (along with unmodified control antibodies) were diluted to ~0.2 mg/ml in 8.1 μl of 1× PBS and then mixed with 0.9 μl of NuPAGE sample-reducing agent and 3 μl of 4× NuPAGE sample loading buffer and heated at 95°C for 5 min. Then, we loaded 10 μl of SeeBlue prestained protein standard as a ladder and 12 μl of the antibody mixtures onto NuPAGE 4 to 12% bis-tris mini protein gels and ran them for 35 min at 200 V with 1× NuPAGE MES SDS running buffer. The gels were stained for 30 min with SimplyBlue SafeStain and then destained for up to 2 hours in water before imaging. An increase in the molecular weight of all bands corresponding to DNA-modified heavy chains indicated that all DNA present on the antibody-DNA conjugate had been ligated. This ligation was specific and was not observed in controls where either T4 ligase or the scaffold-complement was not added (fig. S3).

Last, the ligated antibody-switches were modified with Alexa Fluor 546 NHS ester. 15 mM Alexa Fluor 546 NHS ester in DMF was added to 145 nM antibody-switch in 1× PBS to a final fluorophore concentration of 60 μM dye; this reaction was adjusted to pH 9 with 1 M sodium bicarbonate. This mixture was incubated at room temperature for 1 hour and then quenched by adding 33% by volume of 200 mM tris-HCl (pH 7.5). This resulted in a final antibody-switch concentration of ~110 nM.

The antibody-switches contain a site-specific biotin moiety within the DNA scaffold and thus can be directly immobilized onto streptavidin-coated surfaces. For each replicate flow cytometry experiment, immobilization was achieved by suspending 1 μl of streptavidin-coated Dynabeads T1 in 500 μl of 14.5 nM antibody-switch in physiological buffer. For the fiber-optic biosensor experiments, the streptavidin-functionalized fiber sensor tip was immersed in 40 μl of 75 nM antibody-switch in physiological buffer within the measurement chamber. In both cases, the sensor surfaces were incubated for 1 hour at room temperature, washed with physiological buffer, and then incubated in 5 mM BS3 crosslinker in physiological buffer (500 μl for bead-based assays and 40 μl for fiber-based assays) for 30 min to covalently link the antibody-switches to the sensor surface. The beads or fibers were then washed again and incubated in physiological buffer with 5 mM $MgCl_2$ and 200 nM scaffold-complement DNA (500 μl for bead-based assays and 40 μl for fiber-based assays) for 2 hours at room temperature and then overnight at 4°C. Scaffold-complement was added to ensure that the DNA scaffold assumes a double-stranded form. Last, the beads or fiber sensor were washed and resuspended in physiological buffer (500 μl for bead-based assays and 40 μl for fiber-based assays) before testing.

### Flow cytometry testing of antibody-switch binding, reversibility, and kinetics

Antibody-switch binding responses were measured in physiological buffer or 0.45-μm filtered chicken plasma. For each replicate curve within a binding curve experiment, a sample of antibody-switch

beads (500 μl, prepared as described above) was diluted to 2.8 ml of buffer or plasma per replicate binding curve, and then 194 μl of the resulting bead stock was mixed with 6.6 μl of 100 mM DIG or cortisol in DMSO, yielding samples containing 0 to 3.3 mM target. For antibody-switch specificity testing, the same density and volume of beads was incubated with either 1 or 100 μM cortisol, corticosterone, DIG, prednisolone, or progesterone in 0.1% DMSO. These samples were incubated for 1 hour at room temperature to equilibrate before analysis on a cell sorter. To monitor FRET signaling, antibody-switches were excited using a 561-nm laser; donor fluorophore (Alexa Fluor 546) emission was measured using one bandpass filter (583-nm center wavelength and 30-nm bandpass width) and acceptor fluorophore (Cy5 or ATTO643) emission was measured using another bandpass filter (665-nm center wavelength and 30 nm bandpass width). All samples were run to record 3000 to 10,000 bead counts.

To measure the reversibility of the switch responses, we tested the response of switch-coated beads over three cycles of target addition and washing. Thus, to study the switch behavior over these cycles, we tested the beads under seven conditions: before adding target, after target addition 1, after wash 1, after target addition 2, after wash 2, after target addition 3, and after wash 3. We recorded three replicates of this series of seven conditions. To prepare each replicate, a sample of antibody-switch–coupled beads (500 μl, prepared as described above) was diluted into 1.5 ml of physiological buffer and then split into seven different 200 μl of samples to be tested under each of the seven conditions. Switches were subjected to alternating 30-min cycles of incubation at room temperature in physiological buffer containing either 0 or 1 mM DIG/cortisol. To control for the bleaching or degradation of the antibody-switch–coated bead surface over many cycles of removing and adding new wash or target solution to the beads, we ensured that all seven conditions underwent the same number of solution removal and addition steps while varying the number and sequence of wash and target steps to achieve the seven desired conditions. All samples were subjected to a single removal and addition of solution at each time step, with the identity of the solution added (either target-free buffer or 1 mM target) specified in table S2.

To measure the on-rate kinetics of switching using flow cytometry, a sample of antibody-switch–coated beads (500 μl, prepared as described above) was diluted to 3 ml in physiological buffer and then split into three different 1-ml replicates, which were then swapped into 1 ml of buffer containing 1 mM target to measure their kinetic response. To measure the off-rate response, an identical set of bead samples was prepared but then equilibrated in 1 ml of 1 mM target in buffer, followed by swapping them into target-free buffer and subsequently measuring their kinetic response. In both cases, the switch response was measured at 2- to 5-min intervals after changing concentrations with no additional washes.

### Processing and normalization of binding data

All flow cytometry data were processed in FlowJo 10. Bead populations corresponding to singlet beads were selected, and the median fluorescence of each channel within this population was recorded. All data analysis was performed in Microsoft Excel and GraphPad Prism 8.0.2. All flow cytometry data were corrected for background signal by subtracting fluorescence measurements obtained from unmodified beads run on the flow cytometer at the same settings. For all FRET-based flow cytometry data, donor fluorescent emission ($F_{\mathrm{Donor}}$) and acceptor fluorescent emission ($F_{\mathrm{Acceptor}}$) versus target concentration ([Target]; corresponds to either DIG or cortisol depending on dataset), the FRET ratio for each data point was calculated as

$$\frac{F_{\mathrm{Acceptor}}}{\mathrm{F}_{\mathrm{Donor}} + F_{\mathrm{Acceptor}}} \tag{1}$$

Flow cytometry data were normalized to correct for experiment-to-experiment variations in fluorescent intensity due to changes in instrument gain, bead surface density, and photobleaching between replicates and to allow easier visual comparison between different conditions and switches. Normalization was only done by setting a single point to a value of 1, rather than forcing the entire binding curve to span a range of 0 to 1, to maintain a quantitative comparison of the dynamic range and signal of each experiment. Non-normalized FRET ratios and raw FRET data (donor and FRET channels independently) are provided in figs. S4 and S5. Normalization was carried out per replicate for all binding curves. For unlinked binding data (Figs. 2, B and C, and 4, B and C, and fig. S1), binding curves were normalized by setting the largest value in the dataset equal to 1. For antibody-switch binding data (Figs. 2E, 3, and 4, D to F), normalization was done by setting the first FRET measurement in each dataset (either [Target] = 0 or time = 0) to be equal to 1.

### Fitting binding data to obtain affinities, LOD, ULOQ, and kinetic rates

For Cy5-fluorescence–based measurements of bait-DNA binding and target competition, we analyzed Cy5 emission ($F_{\mathrm{Cy5}}$) versus bait-DNA concentration and free target concentration ([Ligand]). These data were fitted to the Langmuir isotherm as follows

$$F_{\mathrm{Cy5}} = A\frac{[\mathrm{Ligand}]}{K_{\mathrm{D}} + [\mathrm{Ligand}]} + y_0 \tag{2}$$

where $K_{\mathrm{D}}$ is the measured affinity of the interaction and $A$ and $y_0$ correspond to the magnitude and ligand-free background of the binding response, respectively.

When assessing the antibody-switch binding response, a Hill fit was used to fit the binding data and extract an $EC_{50}$ for each switch, which corresponds to the concentration of target at which 50% of the maximum switching signal is achieved. This fitting was achieved by using nonlinear least squares fitting to the Hill equation

$$r_{\mathrm{FRET}} = A\frac{[\mathrm{Target}]^n}{\mathrm{EC}_{50}^n + [\mathrm{Target}]^n} + y_0 \tag{3}$$

where $n$ is the Hill coefficient corresponding to the degree of cooperativity observed during switching. $K_{\mathrm{D}}$ and $EC_{50}$ values are reported as the best-fit value with 95% CI upper and lower bounds from fitting.

LODs were determined from the mean values of $A$, $y_0$, $n$,and $EC_{50}$ as determined from fitting, as well as the SDs ($\sigma$) of these parameters. We applied the standard definition of LOD, which is the target concentration at which the switch response is three SDs above background. Thus, LODs for all switches were determined by solving the equation

$$3\sigma_{y_0} = A\frac{\mathrm{LOD}^n}{\mathrm{EC}_{50}^n + \mathrm{LOD}^n} \tag{4}$$

Upper limits of quantification (ULOQ′s) were determined from the mean values of $A$, $y_0$, $n$, and $EC_{50}$ as determined from fitting, as well as the SDs (σ) of these parameters. The ULOQ is the concentration at which the switch response is three SDs below the saturating signal, which we calculated as follows

$$3\sigma_A = A\frac{ULOQ^n}{EC_{50}^n + ULOQ^n} \quad (5)$$

To determine the kinetics of the on- and off-switching response, we first normalized the FRET ratio ($r_{FRET}$) versus time ($t$) based on the initial measurement and then fitted these data with a single-phase exponential decay model of the form

$$r_{FRET} = (r_{FRET,0} - r_{FRET,f})e^{-t/\tau} + r_{FRET,f} \quad (6)$$

where $r_{FRET,0}$ and $r_{FRET,f}$ are respectively the FRET ratios before and after prolonged laser excitation and τ is the time constant that characterizes the kinetics of antibody-switching behavior.

### Fiber optic measurement system setup

The fiber optic measurement system comprises an optical readout system and tapered fiber optic probe. The development of both components has been thoroughly documented and characterized for continuous sensing in previous work (*33*). Briefly, the optical readout system is designed to excite donor fluorophores on the probe and collect the resulting fluorescent donor and acceptor emission signals, enabling continuous FRET ratio measurements. Excitation light is provided by a 532-nm laser that passes through laser-line filters into a fiber switch. The fiber switch connects either to the sample probe or a dead-end port, allowing measurements with an interval controlled by an Arduino and LabVIEW GUI. When connected, laser light excites the sample probe, and then emission light is coupled back into the reader where it is split into two channels using filters to isolate either donor or acceptor emission. These signals are measured using a single-photon counting module (SPCM) with an integration time of 500 ms and ~300-nW output laser power.

### Preparation of fiber optic tip probes

Fiber optic probes were fabricated as described previously (*33*). Briefly, one end of a graded index multimode fiber (Thorlabs GIF625) was heated and pulled with a Vytran GPX3000 optical fiber processor (Thorlabs) to form tapered fiber probes with a ~10-μm tip and an exposed glass surface. The other end of the fiber is terminated by a standard connector that interfaces with the optical readout system. The exposed glass tip was functionalized using a home-built micro-stage setup to dip controlled lengths of the fiber tip into the various solutions needed for functionalization. We cleaned and hydroxyl-activated the fiber optic tips with piranha solution (25% $H_2O_2$ and 75% concentrated $H_2SO_4$) for 2 hours, followed by two to three washes with ultrapure water and acetone. The fiber tips were incubated in VECTABOND [3% (v/v) in acetone) for 10 min to functionalize the surface with amine groups, then washed with ultrapure water, and dried for 5 min at room temperature. We then coated this surface with a PEG monolayer containing ~2% biotin-terminated PEG for robust attachment of antibody-switches. This was done by incubating the amine-functionalized surface with a mixture of 32% (w/w) Methoxy poly(ethylene glycol) succinimidyl valerate (mPEG-SVA) (MW of 5000) and 0.5% (w/w) biotin-PEG-SVA (MW of 5000) in 0.11 M sodium bicarbonate for 3 hours and then rinsing with water. PEG-functionalized fibers were then placed in 50 μl of flow chambers (Grace Biolabs Hybri-Well Hybridization Cover-HBW6L) mounted onto glass slides to form small measurement chambers with two ports for adding samples during continuous experiments. These chamber-mounted fibers were then stored dry at 4°C for up to a week before use. Before measurement, the fiber surfaces were incubated with 40 μl of (~200 nM; 0.2 mg/ml) streptavidin solution for 10 min and then washed three times with physiological buffer. The CSO-DNA switch was then immobilized onto the fiber sensor surface as described above. Last, the switch-functionalized fiber optic probe was connected to the optical readout system for continuous measurements.

### Fiber optic measurement and data analysis

Continuous fiber-based measurements of the antibody-switch response were performed by measuring the switch response for 5 s (10 points with 500 ms integration time each) at approximately 30-s intervals. During continuous measurement, the sample concentration within the chamber was varied by pipetting samples with differing cortisol concentration into the chamber at noted time intervals (samples used were either physiological buffer described above containing a final concentration of 0.1% DMSO or healthy human donor blood spiked with cortisol to contain a final mixture of 99% blood, ~1% buffer, and >0.1% DMSO). Samples were injected as two 50-μl injections at each time point to ensure full replacement of the fluid within the chamber. After changing the sample within the chamber, the fiber sensor was left in the new sample with no agitation or flow while recording the donor and acceptor emission and using Eq. 1 to calculate the corresponding FRET ratio. Intermittently (every ~1 hour), the laser output power was tested and adjusted to maintain ~300 nW. To correct for the impact of photobleaching, we first performed a 10- to 15-min photobleaching calibration experiment to extrapolate the shift in baseline due to photobleaching over our entire measurement time (fig. S7). We then subtracted the measured FRET ratio from this predicted FRET baseline to obtain the final "inverted" (signal-ON as opposed to signal-OFF) plots shown in Fig. 5.

The kinetics of the antibody-switch response were investigated by first isolating the response of the antibody-switch sensor to all individual sample injections during measurement. Each sensor response from the time of each injection to the time of the next injection was separated and then normalized in signal from 0 to 1, where 0 was the smallest signal value and 1 was the largest. These data are shown in fig. S8 (A and B). These normalized data were then fit with a single exponential as described above for extracting the rate constants of equilibration as a function of final cortisol concentration during equilibration. These rate constants are plotted in fig. S8C. The lack of dependence of the rate constant on the final concentration is consistent with our proposed antibody-switch mechanism, where both on- and off-switching are limited by the kinetics of slow dissociation events (Supplementary Discussion 1).

To account for fiber-to-fiber geometry and signal differences between sensors in replicate experiments (Fig. 5C), we performed single-point calibration of the FRET ratio. Measurements from the green and FRET sensor channels were normalized by dividing the measurements at all time points by the initial reading at $t$ = 0

min in a buffer. This normalization leads to initial measurement signals of green = 1, FRET = 1, and FRET ratio = 0.5. After normalization, photobleaching correction was applied as above using the average photobleaching rate across all replicates. Steady-state sensor responses for assessing the reproducibility of replicates in the physiological range (Fig. 5D) were obtained by averaging the last three measured FRET response values after reaching signal saturation; the solution cortisol concentration was then changed, and the resulting signal was again averaged across $n = 3$ sensors. The steady-state response curve was fitted with the same Hill model as for the bead-binding experiments (Eq. 3), fixing the $EC_{50}$ and $n$ values to match those measured on beads for the same antibody-switch. The predicted LOD was extracted from these measurements using the standard definition described above (Eq. 4). For measurements made in 99% human whole blood (Fig. 6), single-point calibration was performed upon equilibration in unspiked blood to capture signal intensity variations within the unique optical environment of whole blood. No photobleaching correction was applied here, as the measurement duration was shorter and biofouling or drift effects were more substantial than the effects of bleaching.

## Supplementary Materials

**This PDF file includes:**

Supplementary Discussion
Figs. S1 to S11
Tables S1 and S2

## REFERENCES AND NOTES


1. S. S. Gambhir, T. J. Ge, O. Vermesh, R. Spitler, Toward achieving precision health. *Sci. Transl. Med.* **10**, eaao3612 (2018).
2. T. L. Gruenewald, T. E. Seeman, C. D. Ryff, A. S. Karlamangla, B. H. Singer, Combinations of biomarkers predictive of later life mortality. *Proc. Natl. Acad. Sci. U.S.A.* **103**, 14158–14163 (2006).
3. D. H. Hellhammer, S. Wüst, B. M. Kudielka, Salivary cortisol as a biomarker in stress research. *Psychoneuroendocrinology* **34**, 163–171 (2009).
4. M. Vettoretti, G. Cappon, G. Acciaroli, A. Facchinetti, G. Sparacino, Continuous glucose monitoring: Current use in diabetes management and possible future applications. *J. Diabetes Sci. Technol.* **12**, 1064–1071 (2018).
5. J. Kim, A. S. Campbell, B. E.-F. de Ávila, J. Wang, Wearable biosensors for healthcare monitoring. *Nat. Biotechnol.* **37**, 389–406 (2019).
6. A. Kumar, D. Roberts, K. E. Wood, B. Light, J. E. Parrillo, S. Sharma, R. Suppes, D. Feinstein, S. Zanotti, L. Taiberg, D. Gurka, A. Kumar, M. Cheang, Duration of hypotension before initiation of effective antimicrobial therapy is the critical determinant of survival in human septic shock*. *Crit. Care Med.* **34**, 1589–1596 (2006).
7. T. Keller, T. Zeller, D. Peetz, S. Tzikas, A. Roth, E. Czyz, C. Bickel, S. Baldus, A. Warnholtz, M. Fröhlich, C. R. Sinning, M. S. Eleftheriadis, P. S. Wild, R. B. Schnabel, E. Lubos, N. Jachmann, S. Genth-Zotz, F. Post, V. Nicaud, L. Tiret, K. J. Lackner, T. F. Münzel, S. Blankenberg, Sensitive troponin I assay in early diagnosis of acute myocardial infarction. *N. Engl. J. Med.* **361**, 868–877 (2009).
8. H. C. Ates, J. A. Roberts, J. Lipman, A. E. G. Cass, G. A. Urban, C. Dincer, On-site therapeutic drug monitoring. *Trends Biotechnol.* **38**, 1262–1277 (2020).
9. I. B. Hirsch, E. E. Wright Jr., Using flash continuous glucose monitoring in primary practice. *Clin. Diabetes.* **37**, 150–161 (2019).
10. W. H. Polonsky, D. Hessler, K. J. Ruedy, R. W. Beck; DIAMOND Study Group, The impact of continuous glucose monitoring on markers of quality of life in adults with type 1 diabetes: Further findings from the DIAMOND randomized clinical trial. *Diabetes Care* **40**, 736–741 (2017).
11. I. A. Walker, M. Newton, A. T. Bosenberg, Improving surgical safety globally: Pulse oximetry and the WHO Guidelines for Safe Surgery. *Pediatr. Anesth.* **21**, 825–828 (2011).
12. C. Chen, Q. Xie, D. Yang, H. Xiao, Y. Fu, Y. Tan, S. Yao, Recent advances in electrochemical glucose biosensors: A review. *RSC Adv.* **3**, 4473–4491 (2013).
13. A. Jubran, Pulse oximetry. *Crit. Care* **19**, 272 (2015).
14. K. W. Plaxco, H. T. Soh, Switch-based biosensors: A new approach towards real-time, in vivo molecular detection. *Trends Biotechnol.* **29**, 1–5 (2011).
15. Y. Xiao, A. A. Lubin, A. J. Heeger, K. W. Plaxco, Label-free electronic detection of thrombin in blood serum by using an aptamer-based sensor. *Angew. Chem. Int. Ed.* **44**, 5456–5459 (2005).
16. J. S. Swensen, Y. Xiao, B. S. Ferguson, A. A. Lubin, R. Y. Lai, A. J. Heeger, K. W. Plaxco, H. Tom, Continuous, real-time monitoring of cocaine in undiluted blood serum via a microfluidic, electrochemical aptamer-based sensor. *J. Am. Chem. Soc.* **131**, 4262–4266 (2009).
17. B. S. Ferguson, D. A. Hoggarth, D. Maliniak, K. Ploense, R. J. White, N. Woodward, K. Hsieh, A. J. Bonham, M. Eisenstein, T. E. Kippin, K. W. Plaxco, H. T. Soh, Real-time, aptamer-based tracking of circulating therapeutic agents in living animals. *Sci. Transl. Med.* **5**, 213ra165 (2013).
18. N. Nakatsuka, K.-A. Yang, J. M. Abendroth, K. M. Cheung, X. Xu, H. Yang, C. Zhao, B. Zhu, Y. S. Rim, Y. Yang, P. S. Weiss, M. N. Stojanović, A. M. Andrews, Aptamer–field-effect transistors overcome Debye length limitations for small-molecule sensing. *Science* **362**, 319–324 (2018).
19. P. Dauphin-Ducharme, K. Yang, N. Arroyo-Currás, K. L. Ploense, Y. Zhang, J. Gerson, M. Kurnik, T. E. Kippin, M. N. Stojanovic, K. W. Plaxco, Electrochemical aptamer-based sensors for improved therapeutic drug monitoring and high-precision, feedback-controlled drug delivery. *ACS Sens.* **4**, 2832–2837 (2019).
20. B. Wang, C. Zhao, Z. Wang, K. A. Yang, X. Cheng, W. Liu, W. Yu, S. Lin, Y. Zhao, K. M. Cheung, H. Lin, H. Hojaiji, P. S. Weiss, M. N. Stojanović, A. J. Tomiyama, A. M. Andrews, S. Emaminejad, Wearable aptamer-field-effect transistor sensing system for noninvasive cortisol monitoring. *Sci. Adv.* **8**, eabk0967 (2022).
21. D. Wu, C. K. L. Gordon, J. H. Shin, M. Eisenstein, H. T. Soh, Directed evolution of aptamer discovery technologies. *Acc. Chem. Res.* **55**, 685–695 (2022).
22. Z. Tang, P. Mallikaratchy, R. Yang, Y. Kim, Z. Zhu, H. Wang, W. Tan, Aptamer switch probe based on intramolecular displacement. *J. Am. Chem. Soc.* **130**, 11268–11269 (2008).
23. J. Das, S. Gomis, J. B. Chen, H. Yousefi, S. Ahmed, A. Mahmud, W. Zhou, E. H. Sargent, S. O. Kelley, Reagentless biomolecular analysis using a molecular pendulum. *Nat. Chem.* **13**, 428–434 (2021).
24. N. Maganzini, A. Reschke, A. Cartwright, Y. Gidi, I. A. P. Thompson, A. Hariri, C. Dory, Y. Rosenberg-Hasson, J. Pan, M. Eisenstein, T. T. Cornell, H. T. Soh, A rapid ELISA platform with no sample preparation requirement. 2023.04.14.536923 (2023). https://doi.org/10.1101/2023.04.14.536923.
25. F. Ricci, A. Vallée-Bélisle, A. J. Simon, A. Porchetta, K. W. Plaxco, Using nature's "Tricks" to rationally tune the binding properties of biomolecular receptors. *Acc. Chem. Res.* **49**, 1884–1892 (2016).
26. N. Maganzini, I. Thompson, B. Wilson, H. T. Soh, Pre-equilibrium biosensors as an approach towards rapid and continuous molecular measurements. *Nat. Commun.* **13**, 7072 (2022).
27. M. Kadmiel, J. A. Cidlowski, Glucocorticoid receptor signaling in health and disease. *Trends Pharmacol. Sci.* **34**, 518–530 (2013).
28. L. Thau, J. Gandhi, S. Sharma, "Physiology, Cortisol" in *StatPearls* (StatPearls Publishing, Treasure Island (FL), 2022; http://www.ncbi.nlm.nih.gov/books/NBK538239/).
29. R. C. Bhake, V. Kluckner, H. Stassen, G. M. Russell, J. Leendertz, K. Stevens, A. C. E. Linthorst, S. L. Lightman, Continuous free cortisol profiles—circadian rhythms in healthy men. *J. Clin. Endocrinol. Metab.* **104**, 5935–5947 (2019).
30. R. V. Carsia, "Chapter 26 - Adrenals" in *Sturkie's Avian Physiology (Sixth Edition)*, C. G. Scanes, Ed. (Academic Press, San Diego, 2015; https://www.sciencedirect.com/science/article/pii/B9780124071605000269), pp. 577–611.
31. J. G. Lewis, C. J. Bagley, P. A. Elder, A. W. Bachmann, D. J. Torpy, Plasma free cortisol fraction reflects levels of functioning corticosteroid-binding globulin. *Clin. Chim. Acta* **359**, 189–194 (2005).
32. G. L. Hammond, Plasma steroid-binding proteins: Primary gatekeepers of steroid hormone action. *J. Endocrinol.* **230**, R13–R25 (2016).
33. A. A. Hariri, A. P. Cartwright, C. Dory, Y. Gidi, S. Yee, K. X. Fu, K. Yang, D. Wu, I. A. P. Thompson, N. Maganzini, T. Feagin, B. E. Young, B. H. Afshar, M. Eisenstein, M. Digonnet, J. Vuckovic, H. T. Soh, Continuous optical detection of small-molecule analytes in complex biomatrices. bioRxiv 5310304 [Preprint]. 6 March 2023. https://doi.org/10.1101/2023.03.03.531030.
34. G. P. Forlenza, T. Kushner, L. H. Messer, R. P. Wadwa, S. Sankaranarayanan, Factory-calibrated continuous glucose monitoring: How and why it works, and the dangers of reuse beyond approved duration of wear. *Diabetes Technol. Ther.* **21**, 222–229 (2019).
35. S. Somasundaram, C. J. Easley, A nucleic acid nanostructure built through on-electrode ligation for electrochemical detection of a broad range of analytes. *J. Am. Chem. Soc.* **141**, 11721–11726 (2019).
36. N. Khuda, S. Somasundaram, C. J. Easley, Electrochemical sensing of the peptide drug exendin-4 using a versatile nucleic acid nanostructure. *ACS Sens.* **7**, 784–789 (2022).

37. A. Gurukandure, S. Somasundaram, A. S. N. Kurian, N. Khuda, C. J. Easley, Building a nucleic acid nanostructure with DNA-epitope conjugates for a versatile electrochemical protein detection platform (2023). doi:10.26434/chemrxiv-2023-bg1f9.
38. D. Kang, S. Sun, M. Kurnik, D. Morales, F. W. Dahlquist, K. W. Plaxco, New architecture for reagentless, protein-based electrochemical biosensors. *J. Am. Chem. Soc.* **139**, 12113–12116 (2017).
39. E. W. A. Visser, J. Yan, L. J. van IJzendoorn, M. W. J. Prins, Continuous biomarker monitoring by particle mobility sensing with single molecule resolution. *Nat. Commun.* **9**, 2541 (2018).
40. L. van Smeden, A. Saris, K. Sergelen, A. M. de Jong, J. Yan, M. W. J. Prins, Reversible immunosensor for the continuous monitoring of cortisol in blood plasma sampled with microdialysis. *ACS Sens.* **7**, 3041–3048 (2022).
41. R. M. Lubken, A. M. de Jong, M. W. J. Prins, Real-time monitoring of biomolecules: Dynamic response limits of affinity-based sensors. *ACS Sens.* **7**, 286–295 (2022).
42. N. Arroyo-Currás, J. Somerson, P. A. Vieira, K. L. Ploense, T. E. Kippin, K. W. Plaxco, Real-time measurement of small molecules directly in awake, ambulatory animals. *Proc. Natl. Acad. Sci. U.S.A.* **114**, 645–650 (2017).
43. D. Chan, J.-C. Chien, E. Axpe, L. Blankemeier, S. W. Baker, S. Swaminathan, V. A. Piunova, D. Y. Zubarev, C. L. Maikawa, A. K. Grosskopf, J. L. Mann, H. T. Soh, E. A. Appel, Combinatorial polyacrylamide hydrogels for preventing biofouling on implantable biosensors. *Adv. Mater.* **34**, 2109764 (2022).
44. Z. Watkins, A. Karajic, T. Young, R. White, J. Heikenfeld, Week-long operation of electrochemical aptamer sensors: New insights into self-assembled monolayer degradation mechanisms and solutions for stability in serum at body temperature. *ACS Sens.* **8**, 1119–1131 (2023).
45. A. Hauke, L. S. S. Kumar, M. Y. Kim, J. Pegan, M. Khine, H. Li, K. W. Plaxco, J. Heikenfeld, Superwetting and aptamer functionalized shrink-induced high surface area electrochemical sensors. *Biosens. Bioelectron.* **94**, 438–442 (2017).
46. J.-W. Seo, K. Fu, S. Correa, M. Eisenstein, E. A. Appel, H. T. Soh, Real-time monitoring of drug pharmacokinetics within tumor tissue in live animals. *Sci. Adv.* **8**, eabk2901 (2022).
47. R. Dorey, C. Piérard, S. Shinkaruk, C. Tronche, F. Chauveau, M. Baudonnat, D. Béracochéa, Membrane mineralocorticoid but not glucocorticoid receptors of the dorsal hippocampus mediate the rapid effects of corticosterone on memory retrieval. *Neuropsychopharmacology* **36**, 2639–2649 (2011).
48. S. I. Presolski, V. P. Hong, M. G. Finn, Copper-catalyzed azide–alkyne click chemistry for bioconjugation. *Curr. Protoc. Chem. Biol.* **3**, 153–162 (2011).
49. B. D. Wilson, A. A. Hariri, I. A. P. Thompson, M. Eisenstein, H. T. Soh, Independent control of the thermodynamic and kinetic properties of aptamer switches. *Nat. Commun.* **10**, 5079 (2019).
50. J. P. Landry, Y. Ke, G.-L. Yu, X. D. Zhu, Measuring affinity constants of 1450 monoclonal antibodies to peptide targets with a microarray-based label-free assay platform. *J. Immunol. Methods* **417**, 86–96 (2015).


**Acknowledgments:** We thank Y. Sun for the assistance with oligonucleotide synthesis and T. Trinh for the assistance with HPLC purification of DNA. **Funding:** This work was supported by the Chan-Zuckerberg Biohub, the Helmsley Trust, and the Wellcome LEAP SAVE program. I.A.P.T. was supported by the Medtronic Foundation Stanford Graduate Fellowship and the Natural Sciences and Engineering Research Council of Canada (NSERC, 416353855). A.A.H. acknowledges support from the Sanjiv Sam Gambhir–Philips Fellowship Program in Precision Health and the NSERC Postdoctoral Fellowships (PDF; Canada). A.P.C. acknowledges support from the NSF Graduate Research Fellowship Program and the Stanford Graduate Fellowship. This work was also supported by the Vincent Coates Foundation Mass Spectrometry Laboratory, Stanford University Mass Spectrometry (RRID:SCR_017801) using the Bruker Microflex MALDI-TOF mass spectrometer (RRID:SCR_018696). **Author contributions:** I.A.P.T., J.P., and H.T.S. devised the initial concept. I.A.P.T. devised the design and synthesis of the DIG-responsive antibody-switch. I.A.P.T, J.S., and L.Z. designed and synthesized the cortisol-responsive antibody-switch. I.A.P.T and J.S. designed, executed, and analyzed data from flow cytometry experiments for the DIG and cortisol switches. I.A.P.T., A.A.H., N.M., A.P.C., S.Y., C.D., and J.V. designed fiber optic real-time sensing experiments and instrumentation. I.A.P.T. executed and analyzed data from fiber optic real-time sensing experiments. I.A.P.T. and H.T.S. wrote the manuscript. J.S., A.A.H., J.P., and M.E. edited and discussed the manuscript. All authors approved the manuscript. **Competing interests:** J.P., I.A.P.T., H.T.S., and N.M. are coinventors on a pending patent application related to this work filed at the World Intellectual Property Organization (no. WO 2022/081541 A1, filed 12 October 2021). A.A.H., C.D., A.P.C., J.V., and H.T.S. are coinventors on a pending patent application related to this work filed at the U.S. Patent and Trademark Office (no. US 2021/0372929 A1, filed 23 October 2019). All other authors declare that they have no competing interests. **Data and materials availability:** All data needed to evaluate the conclusions in the paper are present in the paper and/or the Supplementary Materials.

Submitted 7 March 2023
Accepted 22 August 2023
Published 22 September 2023
10.1126/sciadv.adh4978

Science Advances

# An antibody-based molecular switch for continuous small-molecule biosensing

Ian A.P. Thompson, Jason Saunders, Liwei Zheng, Amani A. Hariri, Nicolò Maganzini, Alyssa P. Cartwright, Jing Pan, Steven Yee, Constantin Dory, Michael Eisenstein, Jelena Vuckovic, and Hyongsok Tom Soh

*Sci. Adv.* **9** (38), eadh4978. DOI: 10.1126/sciadv.adh4978



*Science Advances* (ISSN 2375-2548) is published by the American Association for the Advancement of Science. 1200 New York Avenue NW, Washington, DC 20005. The title *Science Advances* is a registered trademark of AAAS.